CrossMark

Excellent Electroactivity of Ternary Pd–Ag–Sn Nanocatalysts for Ethanol Oxidation

Yuanyuan Zhang[1] · Qingfeng Yi[1] · Zhongliang Deng[1] · Xiulin Zhou[1] · Huidong Nie[1]

Abstract

Multi-walled carbon nanotube (CNT) supported Pd–Ag–Sn nanocatalysts including Pd/CNT, Pd_7Ag_3/CNT, Pd_7Sn_2/CNT, $Pd_7Ag_1Sn_2$/CNT, $Pd_7Ag_2Sn_2$/CNT and $Pd_7Ag_3Sn_2$/CNT, have been prepared in a mixture solution of ethylene glycol and water by $NaBH_4$ reduction method. The samples have been characterized by using scanning electron microscopy, transmission election microscopy, X-ray diffraction, and X-ray photoelectron spectroscopy. Compared to the Pd/CNT and Pd_7Ag_3/CNT catalysts, metal particles of the ternary $Pd_7Ag_2Sn_2$/CNT catalyst are more uniformly dispersed on the surface of CNTs and present the size of ca. 2.4 nm. Both binary Pd–Ag and ternary Pd–Ag–Sn catalysts exhibit the alloying of Pd and Ag. Electrochemical activities of the prepared catalysts for ethanol oxidation in alkaline media were investigated by cyclic voltammetry (CV), chronoamperometry (CA) and electrochemical impedance spectroscopy. Results show that $Pd_7Ag_2Sn_2$/CNT catalyst reveals the highest current density of ethanol oxidation among the prepared catalysts and presents a high steady-state current density for ethanol oxidation from CA measurement, which is 33 times higher than the commercial Pd/C. Also, $Pd_7Ag_2Sn_2$/CNT and $Pd_7Ag_3Sn_2$/CNT catalysts show a large ethanol oxidation peak current density (against Pd loading) of 2.29 and 2.30 A mg^{-1}, indicating the high usage efficiency of Pd particles for ethanol oxidation.

Graphical Abstract
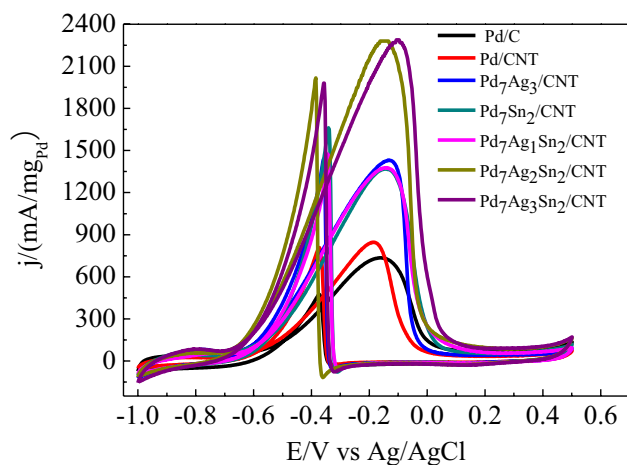
✉ Qingfeng Yi
  yqfyy2001@hnust.edu.cn

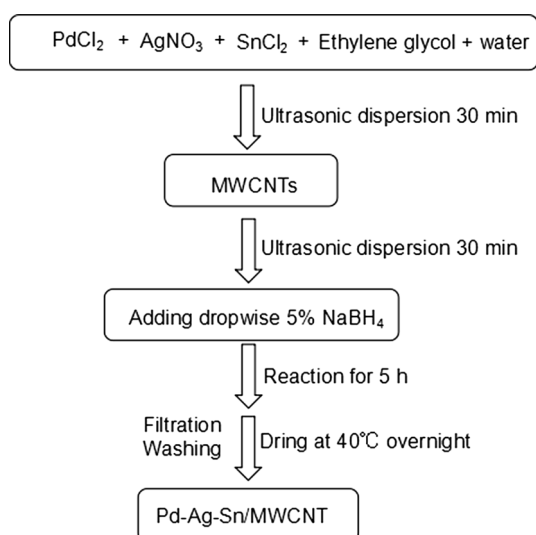Extended author information available on the last page of the article

1 Introduction

The extensive use of traditional fossil fuels leads to the serious pollution of the environment, forcing scientists to research and develop new environment-friendly energy sources. Direct alcohol fuel cells (DAFC) using alcohols as fuels have attracted extensive attention due to much higher energy density of DAFC, easier storage and safer transportation of liquid alcohol fuels than gaseous fuel cell such as H_2/O_2 fuel cell [1–3]. Among the various liquid alcohol fuels, ethanol is preferred as a fuel for direct alcohol fuel cells due to its wide range of sources, less toxicity, easy storage and high energy density [4–6]. In order to ensure the stable and efficient operation of a direct ethanol fuel cell (DEFC), effective electrochemical oxidation of ethanol is one of the most important factors affecting the performance of the DEFC [7]. Pt and Pt-based catalysts including Pt/C [8–10], Pt–M (M = Sn, Ni, Cu) [11–15] and Pt-metal oxide [16–18] were demonstrated to be excellent catalysts for the oxidation of alcohols in both alkaline and acidic media. However, taking into account the expensive price and limited resources of metal Pt, Pt and Pt-based catalysts are greatly hindered in the application of alcohol fuel cells. For the sake of reducing the cost of the catalysts, development of Pt-free catalysts has already become one of the inescapable significant tasks in the study of direct alcohol fuel cells. Pd has proved to show higher electroactivity and better steady-state behavior for ethanol oxidation in alkaline medium than Pt [19–25]. Furthermore, it is well known that the abundance of metal Pd on earth is at least 50 times larger than that of Pt, so Pd is a promising alternative electrocatalyst used to catalyze ethanol oxidation in alkaline media [26, 27]. Liu et al. [2] prepared manganese dioxide coated graphene nanoribbons supported palladium nanoparticles, which exhibited the highest activity and durability towards ethanol oxidation in alkaline media. In addition, considerable efforts have been made to improve the electrocatalytic performance of Pd for ethanol oxidation by adding some other metal or metal oxide to form Pd-based composite catalysts or alloys to increase the active sites of Pd [28–30]. A range of binary and ternary Pd-based catalysts have been synthesized and evaluated, such as binary Pd–Sn [31–33], Pd–Ni [34–36], Pd–Ag [37–39] and ternary Pd–Sn–Ni [29, 40]. Typically, Mao et al. [41] reported the preparation of carbon-supported PdSn–SnO$_2$ catalyst by an impregnation reduction method and found that the catalyst exhibited higher electrocatalytic activity for ethanol oxidation in alkaline solution than that of Pd/C. Ethanol oxidation current density on the PdSn–SnO$_2$ was 68.71 mA cm^{-2} while that on Pd/C was only 28.6 mA cm^{-2}, indicating that the addition of the metal Sn enhanced the electrocatalytic

activity of the Pd catalyst for ethanol oxidation. Dutta et al. [42] prepared the Pd–Au–Ni catalyst grown on a carbon support by chemical reduction of the respective precursors, and the prepared ternary catalyst displayed the ethanol oxidation current density of 159 mA cm^{-2}, which was much higher than pure Pd catalyst. Development of novel Pd-based composite catalysts with stable and efficient electroactivity for ethanol oxidation, therefore, is still a significant work for the study of DEFC.

In this work, multi-walled carbon nanotube (CNT) supported Pd, binary Pd–Ag and ternary Pd–Ag–Sn nanocatalysts with different atomic molar ratios were fabricated and their electroactivity for ethanol oxidation was evaluated in alkaline media. The present results involve the analyses on the morphological texture and surface compositions of the prepared catalysts by X-ray diffraction (XRD), scanning electron microscopy (SEM), transmission election microscopy (TEM) and X-ray photoelectron spectroscopic (XPS) techniques, and the electroactivity measurements by conventional electrochemical techniques.

2 Experimental

The chemicals used in this work included sodium hydroxide, palladium chloride, silver nitrate, stannous chloride, sodium borohydride, ethylene–glycol and ethanol. The chemicals were analytical grade and used as received without further purification. Water was deionized water subjected to the double distillation. Multi-walled CNT were purchased from Aladdin (> 90%, OD: 10–20 nm, length: 5–20 μm). CNT particles were pretreated as follows before they were used to synthesize the catalysts. CNTs were added to a mixture of concentrated H_2SO_4 and concentrated HNO_3 (the volume ratio was 3:1), and the black suspension was then heated and refluxed at 60 °C for 8 h to obtain the acidified CNTs. The $Pd_xAg_ySn_z$/CNT catalysts (x:y:z was the mole ratio of Pd:Ag:Sn) were prepared by the conventional NaBH$_4$ reduction method [29]. A typical synthesis procedure for the $Pd_7Ag_1Sn_2$/CNT (the mole ratio is 7:1:2) was presented in Scheme 1. In detail, 8.9 mg PdCl$_2$, 1.2 mg AgNO$_3$, and 3.2 mg SnCl$_2$ were mixed in the mixed solvent of 12 mL ethylene glycol and 4 mL water, followed by ultrasonication for 30 min to make the solids be totally dissolved. To the formed solution, 30 mg of the acidified CNTs was added and the mixture was ultrasonicated for 30 min to obtain a uniform suspension. Then, 3 mL of 5% NaBH$_4$ dissolved in ethylene glycol was added dropwise under stirring. The chemical reaction was carried out for 5 h and then filtered. The black solid was washed with water, and finally dried under vacuum at 40 °C overnight to obtain the catalyst $Pd_7Ag_1Sn_2$/CNT. In accordance with the same procedure, Pd/CNT (x = 8.9 mg, y = 0 mg and z = 0 mg), Pd_7Ag_3/CNT (x = 8.9 mg, y = 3.6 mg

```
┌─────────────────────────────────────────────┐
│ PdCl₂ + AgNO₃ + SnCl₂ + Ethylene glycol + water │
└─────────────────────────────────────────────┘
                    ⇓ Ultrasonic dispersion 30 min
              ┌──────────┐
              │  MWCNTs  │
              └──────────┘
                    ⇓ Ultrasonic dispersion 30 min
        ┌──────────────────────────┐
        │ Adding dropwise 5% NaBH₄ │
        └──────────────────────────┘
                    ⇓ Reaction for 5 h
    Filtration
    Washing     ⇓ Dring at 40℃ overnight
         ┌──────────────────┐
         │  Pd-Ag-Sn/MWCNT  │
         └──────────────────┘
```

Scheme 1 Preparation procedure of the nanocatalysts

and z = 0 mg), Pd_7Sn_2/CNT (x = 8.9 mg, y = 3.2 mg and z = 0 mg), $Pd_7Ag_2Sn_2$/CNT (x = 8.9 mg, y = 2.4 mg and z = 3.2 mg) and $Pd_7Ag_3Sn_2$/CNT (x = 8.9 mg, y = 3.6 mg and z = 3.2 mg) were synthesized by adjusting the molar ratio of metal precursors.

Compositions of the prepared catalysts were analyzed by XRD obtained in a D/MAX2500X diffractometer (Japan), operating with Cu K alpha radiation generated at 40 kV and 250 mA (l = 0.15418 nm). Surface morphological textures of the samples were characterized by SEM and TEM. SEM images were obtained with a field emission scanning electron microscope (Nova NanoSEM230), and TEM images were obtained through a JEM-2100F transmission electron microscopy. Surface electron structures of the prepared catalysts were investigated by XPS analysis obtained with an ESCALAB 250Xi spectrometer (VG Scientific Ltd., England) using Al K_α radiation (1486.6 eV). The Pd mass percentages in the prepared catalysts with respect to the total masses of the catalysts were determined by using inductively coupled plasma (ICP-AES-7510, Shimadzu), and all results were listed in Table 1.

A conventional three-electrode system was used to study the electrochemical activity of the prepared catalysts with AutoLab PGSTAT30/FRA electrochemical workstation (Eco Chimie, The Netherlands). The glassy carbon (GC) electrode modified with the prepared catalysts, Ag/AgCl in saturated KCl solution and Pt foil were used as working, reference and

counter electrode, respectively. All potentials reported in this work were referenced against the Ag/AgCl. The working electrode was fabricated according to the following steps: A GC electrode (3 mm diameter, from LanLiKe, TianJing, China) was polished with a 0.3 μm alumina suspension to give a mirror surface. Then, 5 mg of the catalyst sample was well dispersed in the mixed solution containing 0.94 mL of ethanol and 60 μL of Nafion solution (5 wt% in water) by sonication for 1 h to obtain an ink. 15 μL of this ink was dropped onto the GC surface and dried at room temperature to obtain the working electrode. For the EIS measurements, the range of frequency was controlled from 40 kHz to 40 mHz, and the amplitude of modulation potential was 10 mV. For comparison, electrochemical activity of commercial Pd/C (wt% = 10%, Aladdin) for ethanol oxidation was also investigated. All electrochemical measurements were performed at room temperature.

3 Results and Discussion

Figure 1a–d reveal SEM images of the Pd/CNT, Pd_7Ag_3/CNT, Pd_7Sn_2/CNT and $Pd_7Ag_2Sn_2$/CNT catalysts as the typical samples. It is observed that a large number of nanoparticles are loaded on the staggered arrangement of CNTs for these catalysts. Pd/CNT, Pd_7Ag_3/CNT and Pd_7Sn_2/CNT catalysts exhibit an aggregation between the nanoparticles as shown in Fig. 1a–c. It is clearly seen form Fig. 1d that the catalyst particles of the $Pd_7Ag_2Sn_2$/CNT sample are well uniformly dispersed on the surface of CNTs and no obvious aggregation arises, indicating that the addition of proper amount of Ag and Sn is helpful to improve the dispersibility of Pd catalyst particles.

Figure 2a–d show TEM images of the Pd/CNT, Pd_7Ag_3/CNT, Pd_7Sn_2/CNT and $Pd_7Ag_2Sn_2$/CNT catalysts. Particle size distribution histograms are presented in corresponding TEM image. The Pd/CNT and $Pd_7Ag_2Sn_2$/CNT catalysts particles are uniformly dispersed on the CNT except for a small amount of agglomeration in Fig. 2a, d. According to the distribution histograms as indicated in the insets, the average particle sizes of Pd/CNT and $Pd_7Ag_2Sn_2$/CNT catalysts are 3.6 and 2.4 nm respectively. It is seen from Fig. 2b, c that the particles of the Pd_7Ag_3/CNT and Pd_7Sn_2/CNT catalysts present a relatively larger average diameter of 4.7 and 3.7 nm respectively, due to the presence of agglomeration. Results show that the catalyst particles on $Pd_7Ag_2Sn_2$/CNT display a small size and a well uniform dispersion on

**Table 1** Pd loading of the prepared samples from ICP measurement

Catalysts	Pd/CNT	Pd_7Ag_3/CNT	Pd_7Sn_2/CNT	$Pd_7Ag_1Sn_2$/CNT	$Pd_7Ag_2Sn_2$/CNT	$Pd_7Ag_3Sn_2$/CNT
Pd loading (wt%)	9.95	8.90	8.27	8.33	7.57	6.95

Fig. 1 SEM images of the Pd/CNT (**a**), Pd$_7$Ag$_3$/CNT (**b**), Pd$_7$Sn$_2$/CNT (**c**) and Pd$_7$Ag$_2$Sn$_2$/CNT (**d**) samples
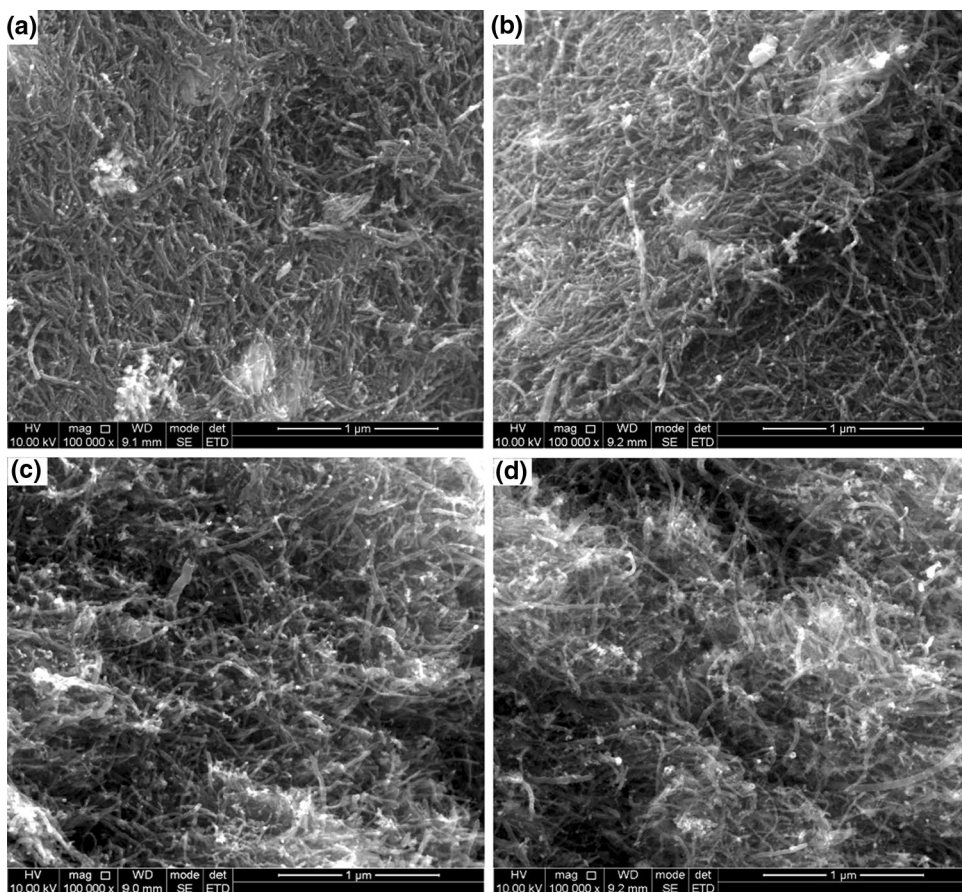
Fig. 2 TEM images and the corresponding size distributions of the Pd/CNT (**a**), Pd$_7$Ag$_3$/CNT (**b**), Pd$_7$Sn$_2$/CNT(**c**) and Pd$_7$Ag$_2$Sn$_2$/CNT (**d**) samples
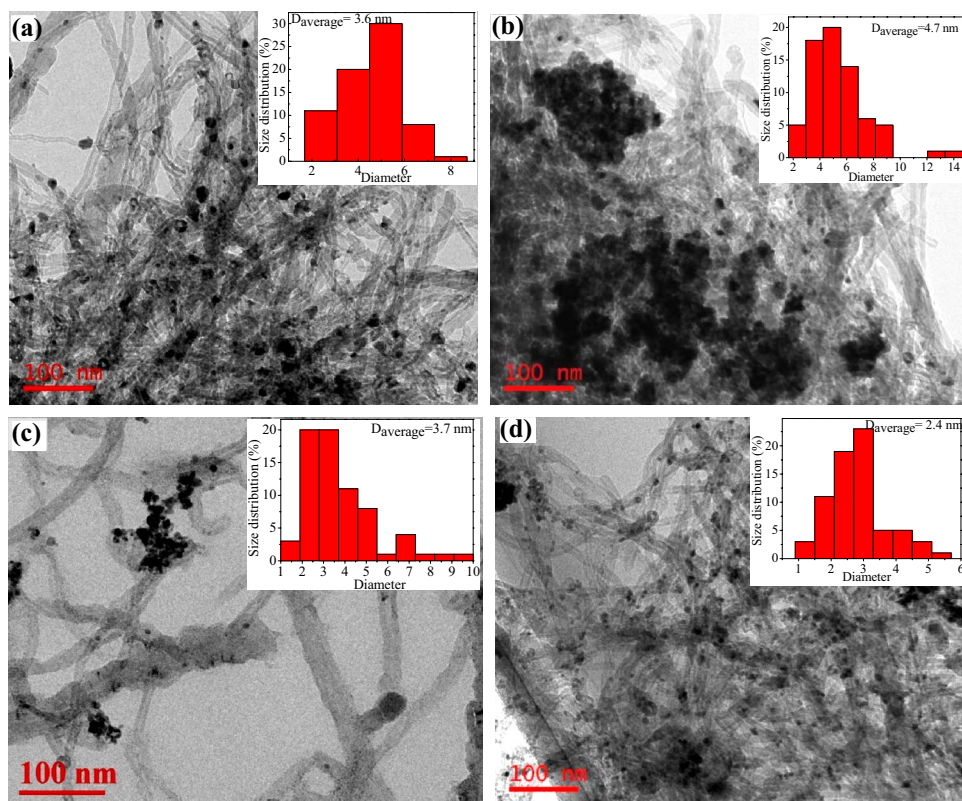
CNTs, which favors for the formation of large numbers of catalytic active sites.

The XRD patterns of the prepared samples are shown in Fig. 3. As can be seen, the diffraction peaks at 25.8° and 54.5° observed for CNT are referred to the hexagonal graphite structures (002) and (004) planes respectively [43]. The Pd/CNT catalyst clearly shows four main characteristic peaks of fcc crystalline Pd at 40.1°, 46.6°, 68.1° and 82.1°, named the planes (111), (200), (220) and (311), respectively. For the Pd_7Ag_3/CNT, $Pd_7Ag_1Sn_2$/CNT, $Pd_7Ag_2Sn_2$/CNT and $Pd_7Ag_3Sn_2$/CNT catalysts, the angle position of the Pd diffraction peaks exhibits a bit negative shift compared with pure Pd catalyst (Pd/CNT), however, the Pd_7Sn_2/CNT catalyst has no significantly shift. This reveals the alloy formation between Pd and Ag for Pd_7Ag_3/CNT and ternary Pd–Ag–Sn catalysts, which is attributed to the incorporation of Ag into the Pd fcc structure. No corresponding diffraction peak of Ag or Sn could be observed in the as-prepared binary and ternary catalysts due to lower concentration levels of Ag and Sn or the possibly poor crystallinity.

The Pd 3d, Ag 3d and Sn 3d core level XPS data of Pd/CNT, Pd_7Ag_3/CNT, Pd_7Sn_2/CNT and $Pd_7Ag_2Sn_2$/CNT catalysts are shown in Fig. 4a–c. The binding energy at 335.7 eV (3d5/2) and 340.4 eV (3d3/2) corresponds to the peak of the metal Pd in the catalysts as indicated in Fig. 4a, and the binding energy of the other two peaks at 337.3 and 342.7 eV is indexed to the Pd oxides due to the exposure of the samples to air, indicating that both metal Pd and Pd oxide are present in the catalysts. The Ag 3d spectra of the as-synthesized Pd_7Ag_3/CNT and $Pd_7Ag_2Sn_2$/CNT samples shown in Fig. 4b present the two peaks centered at 367.9 and 373.9 eV corresponding to Ag 3d5/2 and Ag 3d3/2 respectively, proving that the Ag ion in the solution is completely reduced to Ag element. Moreover, Fig. 4c reveals two peaks located on 487.1 and 495.9 eV contributed to SnO_2 3d5/2

and SnO_2 3d3/2 respectively, reflecting that the metal Sn in the $Pd_7Ag_2Sn_2$/CNT and Pd_7Sn_2/CNT catalysts exists in the form of oxide.

Cyclic voltammetric (CV) data of the prepared catalysts in 1 mol L^1 NaOH solution are shown in Fig. 5. It can be seen from Fig. 5 that a cathode reduction peak (r_c) is observed at the potential of −0.42 to −0.33 V for all the catalysts, which can be attributed to the reduction of Pd oxides produced during the forward potential scan. It can be also observed from Fig. 5 that the r_c peak current density of these reduction peaks on the Pd/C, Pd/CNT, Pd_7Ag_3/CNT, Pd_7Sn_2/CNT, $Pd_7Ag_1Sn_2$/CNT, $Pd_7Ag_2Sn_2$/CNT, $Pd_7Ag_3Sn_2$/CNT catalysts is 14.3, 17.0, 20.5, 24.6, 20.2, 31.4 and 24.0 mA cm^{-2}, respectively. The electrochemical active surface areas (ECSAs) of Pd and Pd-based catalysts can be calculated by the charge of PdO reduction peak in each CV. The corresponding equation is given as follows (1) [44–46]:

$$ECSA = Q/s \times l \qquad (1)$$

where Q is the coulombic charge determined by integrating current peak of PdO reduction, s is the proportionality constant that related charge with area (405 μC cm^{-2}) and l is the electrocatalyst loading (g cm^{-2}) on the GC electrode. According to the Eq. (1), the ECSAs of Pd/C and the prepared catalysts were evaluated and corresponding results are listed in Table 2. The results show that the ternary $Pd_7Ag_2Sn_2$/CNT catalyst possesses the largest ECSA value among the Pd/C and other Pd-based catalysts, indicating that the addition of an appropriate amount of Ag and Sn can improve the electrochemical active surface area of the Pd catalyst. This is consistent with the results observed from SEM and TEM images.

Electrocatalytic activity of the prepared catalysts in 1 mol L^{-1} NaOH solution containing 0.5 mol L^{-1} ethanol was examined by cyclic voltammetry as indicated in Fig. 6. It is clearly seen from Fig. 6 that all catalysts reveal a characteristic anodic peak j_f caused by ethanol oxidation during the forward scan. The j_f peak current density on the Pd/C, Pd/CNT, Pd_7Ag_3/CNT, Pd_7Sn_2/CNT, $Pd_7Ag_1Sn_2$/CNT, $Pd_7Ag_2Sn_2$/CNT and $Pd_7Ag_3Sn_2$/CNT catalysts is 79.4, 91.4, 137.1, 121.1, 123.6, 187.5 and 170.1 mA cm^{-2}, respectively. Compared with the Pd/C and Pd/CNT catalysts, Pd–Ag/CNT and Pd–Ag–Sn/CNT catalysts display the higher anodic peak current density during the forward scan, indicating that both binary Pd–Ag and ternary Pd–Ag–Sn nanocatalysts have excellent electrocatalytic activity for ethanol oxidation. Although all catalysts possess almost the same onset potential (OP) of ca. −0.65 V for ethanol oxidation, the anodic current density in the potential range of OP to the peak (j_f) potential varies greatly for different catalysts, e.g., the current density at −0.35 V on the Pd/C, Pd/CNT, Pd_7Ag_3/CNT, Pd_7Sn_2/CNT, $Pd_7Ag_1Sn_2$/CNT, $Pd_7Ag_2Sn_2$/CNT and
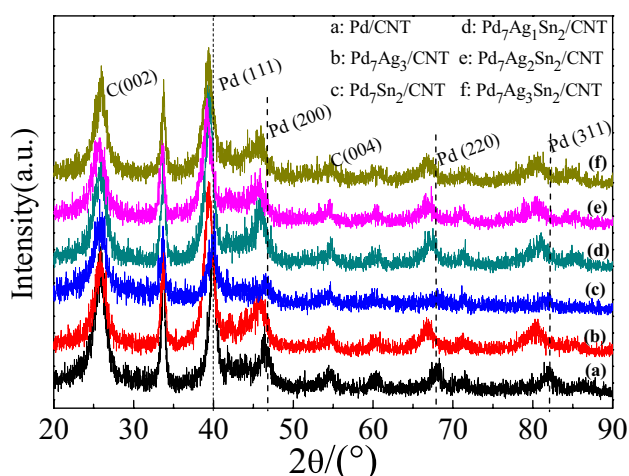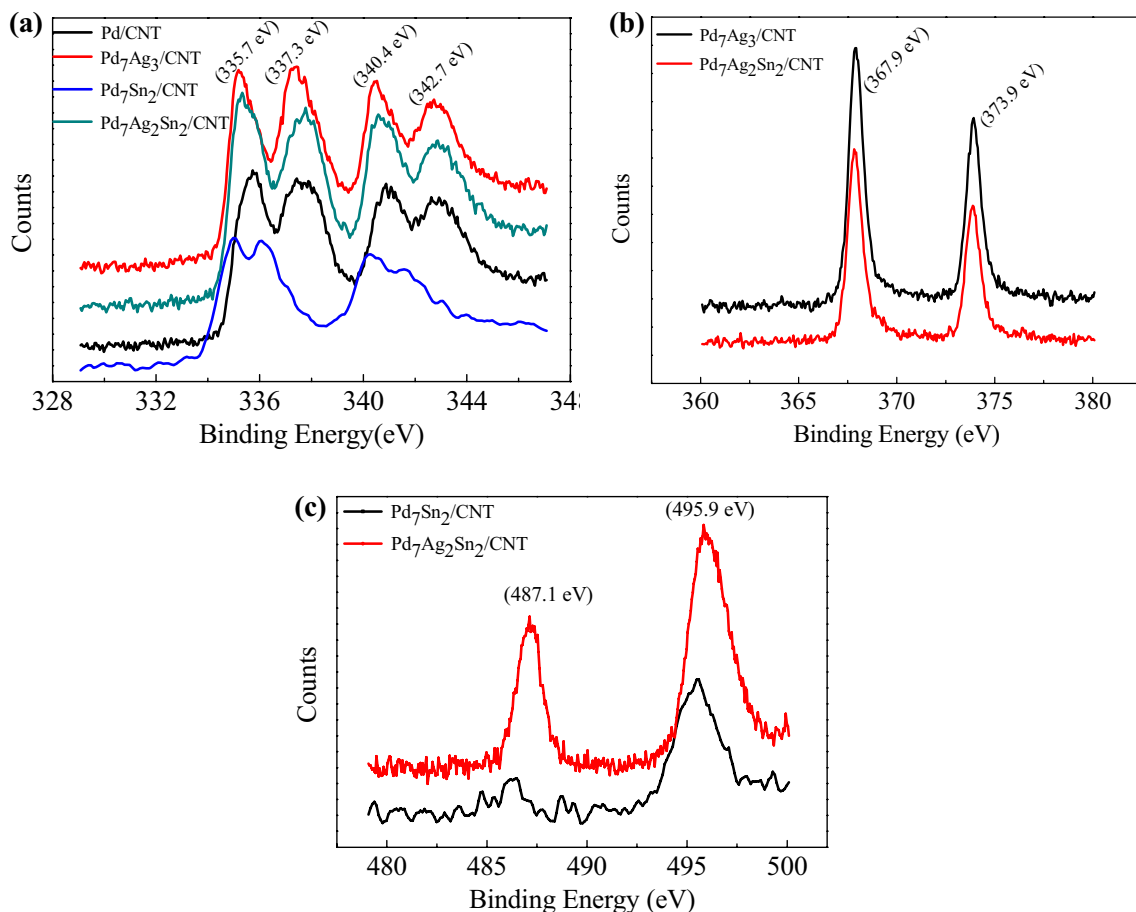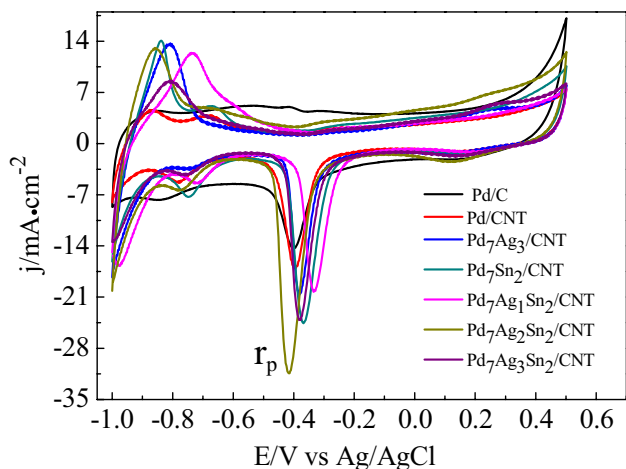

Fig. 3 X-ray diffraction patterns of the prepared samples

Fig. 4 XPS profiles and fitting results of the Pd/CNT, Pd$_7$Ag$_3$/CNT, Pd$_7$Sn$_2$/CNT and Pd$_7$Ag$_2$Sn$_2$/CNT samples: **a** Pd 3d core levels, **b** Ag 3d core levels, **c** Sn 3d core levels
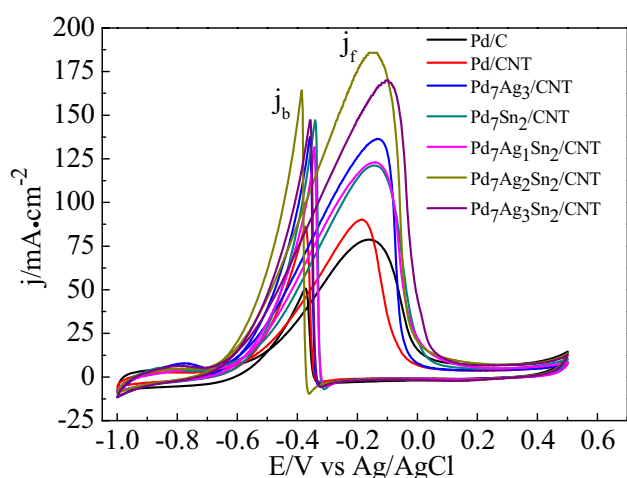

Fig. 5 Cyclic voltammograms of the samples in 1.0 mol L^{-1} NaOH at a scan rate of 50 mV s^{-1}

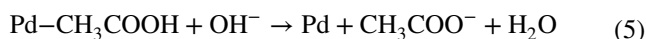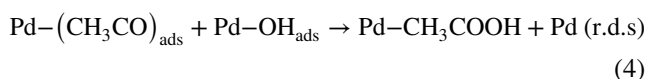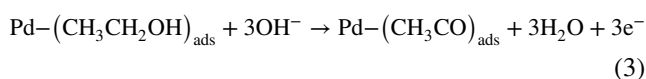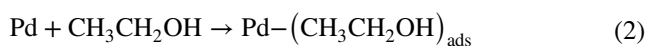**Table 2** ECSA value, Tafel slope and (αn) value of Pd/C and the prepared samples

Catalyst	ECSA (m^2 g^{-1})	Tafel slope (mV dec^{-1})	αn
Pd/C	11.13	169	0.37
Pd/CNT	9.73	127	0.28
Pd$_7$Ag$_3$/CNT	8.75	165	0.36
Pd$_7$Sn$_2$/CNT	11.83	138	0.30
Pd$_7$Ag$_1$Sn$_2$/CNT	9.96	153	0.33
Pd$_7$Ag$_2$Sn$_2$/CNT	15.34	161	0.35
Pd$_7$Ag$_3$Sn$_2$/CNT	11.08	191	0.42

Pd$_7$Ag$_3$Sn$_2$/MWCNT catalysts is 44.2, 51.4, 79.7, 67.1, 73.3, 110.2 and 92.9 mA cm^{-2}, respectively. Results indicate that the reaction rate of ethanol oxidation at the same potential on binary and ternary catalysts is much faster than that on Pd/C and Pd/CNT. This may be related to the synergistic effect between metals. The mechanism for the oxidation of ethanol on Pd follows the Eqs. (2)–(5) [47]:
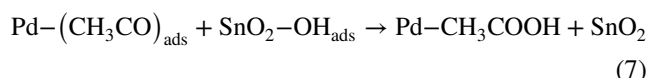
Fig. 6 Cyclic voltammograms of the samples in 1.0 mol L^{-1} NaOH in the presence of 0.5 mol L^{-1} ethanol at a scan rate of 50 mV s^{-1}

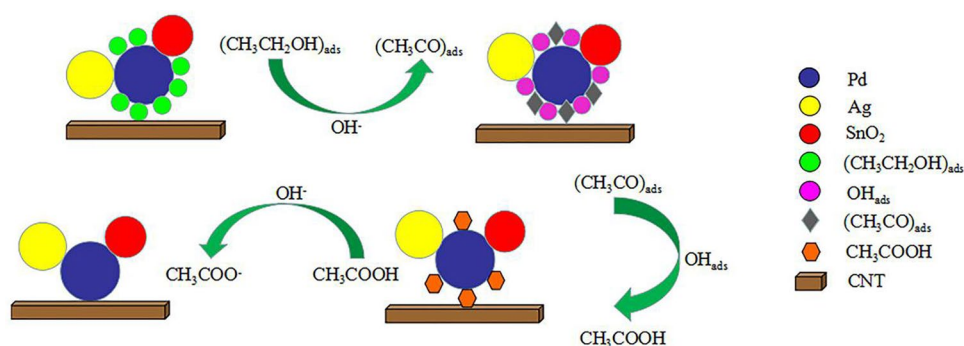catalyst for ethanol oxidation. During the backward-going scan, a well-defined anodic peak (j_b) also arises, caused by the further oxidation of the intermediates formed during the forward-going scan. The ratio between the forward anodic peak current–density (j_f) and the reverse anodic peak current–density (j_b), i.e., j_f/j_b, can be reflected the catalyst tolerance to carbonaceous species accumulation to a extent [44, 48, 49]. The higher j_f/j_b ratio indicates outstanding oxidation of ethanol during the backward scan and less production of carbonaceous species on the surface of the catalyst. The ratio calculated from the Fig. 6 is 1.55, 1.04, 1.00, 0.82, 0.94, 1.15, and 1.16 for the Pd/C, Pd/CNT, Pd$_7$Ag$_3$/CNT, Pd$_7$Sn$_2$/CNT, Pd$_7$Ag$_1$Sn$_2$/CNT, Pd$_7$Ag$_2$Sn$_2$/CNT and Pd$_7$Ag$_3$Sn$_2$/CNT catalysts, respectively. With regard to Pd$_7$Ag$_3$/CNT, Pd$_7$Sn$_2$/CNT and Pd$_7$Ag$_1$Sn$_2$/CNT catalysts, their j_f/j_b ratios are comparatively lower relative to those of other catalysts, reflecting the relaively larger accumulation of carbonaceous intermediates on their surface during ethanol electrooxidation process [30]. Generally, addition of proper amount of one or even two other metals to Pd nanocatalyst can improve its electroactivity. According to the so-called bifunctional mechanism, Pd-Ag bimetallic alloy would be more effective in removing carbonaceous reactive intermediates and releasing the active sites of Pd, and the adsorption of OH$^-$ on the Pd–Ag alloy becomes stronger in view of the *d*-band center theory, which is propitious to enhance the catalytic activity of the catalyst for ethanol oxidation [50]. Furthermore, the metal Sn in the ternary Pd–Ag–Sn catalyst exists in the form of SnO$_2$ by XPS characterization in Fig. 4c. The presence of SnO$_2$ contributes to the adsorption of OH$^-$ on its surface to promote the removal of CO$_{ads}$ adsorbed on Pd [41], leading to accelerate the adsorption and oxidation of ethanol. This can be shown by the following Eqs. (6) and (7) [44]:

$$SnO_2 + OH^- \rightarrow SnO_2-OH_{ads} + e^- \tag{6}$$

$$Pd-\left(CH_3CO\right)_{ads} + SnO_2-OH_{ads} \rightarrow Pd-CH_3COOH + SnO_2 \tag{7}$$

Addition of Ag and SnO$_2$ can therefore, enhance the ability of removing carbonaceous reactive intermediates produced during the oxidation of ethanol and timely release

$$Pd + CH_3CH_2OH \rightarrow Pd-\left(CH_3CH_2OH\right)_{ads} \tag{2}$$

$$Pd-\left(CH_3CH_2OH\right)_{ads} + 3OH^- \rightarrow Pd-\left(CH_3CO\right)_{ads} + 3H_2O + 3e^- \tag{3}$$

$$Pd-\left(CH_3CO\right)_{ads} + Pd-OH_{ads} \rightarrow Pd-CH_3COOH + Pd \ (r.d.s) \tag{4}$$

$$Pd-CH_3COOH + OH^- \rightarrow Pd + CH_3COO^- + H_2O \tag{5}$$

It can be seen from the reactions (2)–(5) that ethanol oxidation is related to the production of both (CH$_3$CO)$_{ads}$ and OH$_{ads}$. Schematic diagram for ethanol oxidation on the ternary Pd–Ag–Sn catalyst is shown in Fig. 7, which involves such main three processes as the adsorption of ethanol molecule on the Pd active sites, the formation of the adsorbed (CH$_3$CO)$_{ads}$ and the production of CH$_3$COO$^-$. At a potential region of < -0.7 V, Pd–(CH$_3$CH$_2$OH)$_{ads}$ species will be formed on the anodic sweep. The CH$_3$CO$_{ads}$ or other carbonaceous reactive intermediates will strongly adsorb on the surface of Pd and block the active sites, which will lead to a decrease in the electrocatalytic activity of the
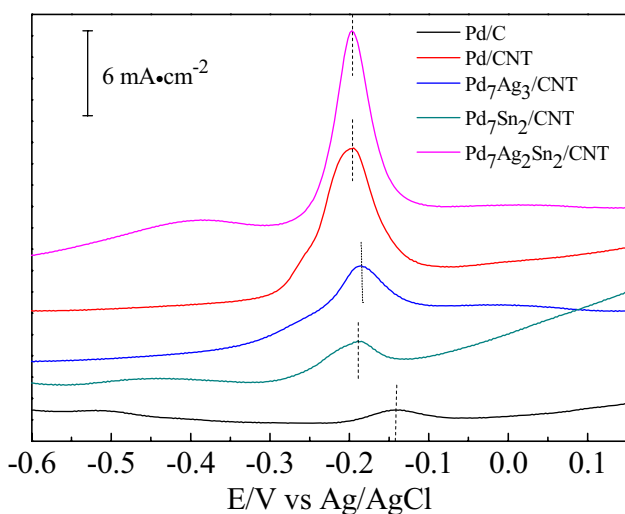
Fig. 7 Schematic diagram for ethanol oxidation on the ternary Pd–Ag–Sn catalyst
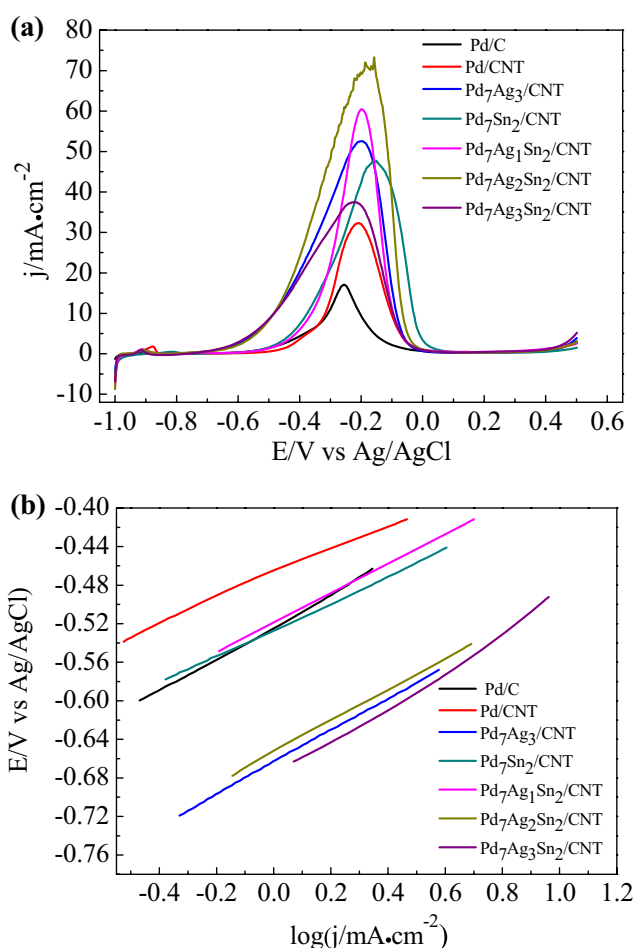
Pd active sites, making the ethanol molecules to rapidly decompose and absorb on the surface of the Pd catalyst. Results show that the ternary Pd–Ag–Sn catalyst can more effectively catalyze the oxidation of ethanol compared to Pd/CNT and Pd/C catalysts.

Although the j_f/j_b ratio can represent the ability of the catalyst to remove organic intermediate species in a degree, compositions of the species are complicated and they may display different adsorption abilities on the catalyst surface. So, the j_f/j_b ratio cannot totally reflect the electroactivity of the catalysts [41, 50]. Generally, carbon monoxide (CO) is used as a typical intermediate substance to measure the anti-poisoning ability of the catalysts. Figure 8 shows the CV curves for the oxidation of pre-adsorbed CO on Pd/C, Pd/CNT, Pd_7Ag_3/CNT, Pd_7Sn_2/CNT and $Pd_7Ag_2Sn_2$/CNT catalysts in 1 mol L^{-1} NaOH solution at 50 mV s^{-1}. The onset potential of CO oxidation on Pd/C, Pd/CNT, Pd_7Ag_3/CNT, Pd_7Sn_2/CNT and $Pd_7Ag_2Sn_2$/CNT catalysts is -0.211, -0.290, -0.310, -0.278 and -0.275 V, respectively, indicating that the oxidation of CO occurs at a more negative potential for the prepared catalysts compared to the Pd/C catalyst. The adsorption of OH^- species on the surface of Pd catalysts is favorable for removal of CO [24]. Therefore, the ability of resistance to CO_{ads} on the prepared catalysts is better than the Pd/C catalyst due to the synergetic effect between Pd and Ag/Sn.

Figure 9a shows the quasi-steady-state polarization curves of ethanol oxidation at the Pd/C and the prepared catalysts at 1 mV s^{-1} in 1 mol L^{-1} NaOH solution in the presence of 0.5 mol L^{-1} ethanol. The peak current density on the ternary $Pd_7Ag_2Sn_2$/CNT catalyst is 71.5 mA cm^{-2}, which is 4.1, 2.2, 1.4 and 1.5 times larger than those on the Pd/C, Pd/CNT, Pd_7Ag_3/CNT and Pd_7Sn_2/CNT catalysts, respectively.


Fig. 9 **a** A quasi-steady-state curves of the ethanol oxidation on the samples in 1.0 mol L^{-1} NaOH in the presence of 0.5 mol L^{-1} ethanol at a scan rate of 1 mV s^{-1}. **b** Tafel plots derived from the curves in (**a**)

Typically, Tafel plots of ethanol oxidation calculated from Fig. 9a were depicted in Fig. 9b. Tafel slope values on Pd/C, Pd/CNT, Pd_7Ag_3/CNT, Pd_7Sn_2/CNT, $Pd_7Ag_1Sn_2$/CNT, $Pd_7Ag_2Sn_2$/CNT and $Pd_7Ag_3Sn_2$/CNT are 169, 127, 165, 138, 153, 161, and 191 mV dec^{-1}, respectively. These similar Tafel slopes reflect that all prepared catalysts have the same reaction mechanism for the ethanol oxidation [51–53]. Butler–Volmer equation is applied to calculate αn, where α is the anodic transfer coefficient and n is the number of transferred electrons. Corresponding results are listed in Table 2. These low αn values imply low α due to infinitesimal change in n values for ethanol oxidation on different catalysts, indicating that the ethanol oxidation process on the prepared catalysts is irreversible.

The catalytic stability of the prepared catalysts was also investigated using chronoamperometric measurement at a constant potential of -0.35 V in 1 mol L^{-1} NaOH solution containing 0.5 mol L^{-1} ethanol as indicated in Fig. 10. Figure 10 reveals that the current density on the Pd/C, Pd/

Fig. 8 CO stripping curves of the samples in 1 mol L^{-1} NaOH at a scan rate of 50 mV s^{-1}
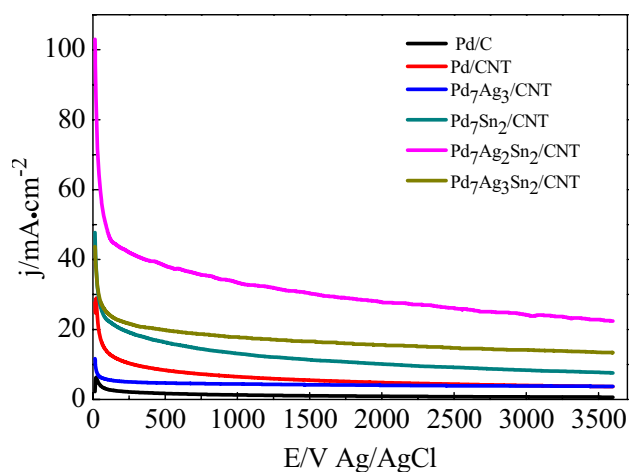
Fig. 10 Chronoamperometric responses of the Pd/C, Pd/CNT, Pd₇Ag₃/CNT, Pd₇Sn₂/CNT, Pd₇Ag₂Sn₂/CNT and Pd₇Ag₃Sn₂/CNT samples in 1.0 mol L^{-1} NaOH in the presence of 0.5 mol L^{-1} ethanol at a constant potential of -0.35 V

CNT, Pd_7Ag_3/CNT, Pd_7Sn_2/CNT, $Pd_7Ag_2Sn_2$/CNT and $Pd_7Ag_3Sn_2$/CNT catalysts is 0.7, 3.7, 4.2, 7.6, 22.6 and 13.3 mA cm^{-2} for the oxidation of ethanol after maintaining 3600 s. It is clear that the $Pd_7Ag_2Sn_2$/CNT catalyst exhibits the highest steady-state current density, which is 32.3, 6.1, 5.4, 2.3 and 1.7 times larger than that observed on the Pd/C, Pd/CNT, Pd_7Ag_3/CNT, Pd_7Sn_2/CNT and $Pd_7Ag_3Sn_2$/CNT catalysts, respectively. Result is consistent with the analysis from the CV data in Fig. 6 and also reveals the excellent electrocatalytic stability of the ternary $Pd_7Ag_2Sn_2$/CNT catalyst for the oxidation of ethanol in alkaline solution.

Electrochemical impedance spectroscopic (EIS) measurements of the samples were carried out in 1 mol L^{-1} NaOH solution in the presence of 0.5 mol L^{-1} ethanol in order to study the electrochemical reaction resistance of ethanol oxidation. Nyquist plots of all samples at the potential of -0.35 V are presented in Fig. 11a. The Nyquist diagrams

of all catalysts show a well semi-circle shape caused by the oxidation of ethanol within the studied frequency range. The impedance values for ethanol oxidation on the Pd/C, Pd/CNT, Pd_7Ag_3/CNT, Pd_7Sn_2/CNT, $Pd_7Ag_1Sn_2$/CNT, $Pd_7Ag_2Sn_2$/CNT and $Pd_7Ag_3Sn_2$/CNT catalysts are 80.3, 75.3, 48.1, 49.2, 61.9, 34.2 and 36.2 ohm, respectively. This can be seen that the $Pd_7Ag_2Sn_2$/CNT catalyst presents the fastest ethanol electro-oxidation rate among the prepared catalysts. The equivalent electric circuit compatible with the Nyquist diagram is shown in Fig. 11b. The fit curves presented in Fig. 11a reveal that the equivalent electric circuit is well consistent with electrochemical processes. The charge transfer resistances of the samples on both the imaginary and real axes follow the order: $Pd_7Ag_2Sn_2$/CNT $< Pd_7Ag_3Sn_2$/CNT $< Pd_7Ag_3$/CNT $< Pd_7Sn_2$/CNT $< Pd_7Ag_1Sn_2$/CNT $<$ Pd/CNT $<$ Pd/C, indicating that their electroactivity towards ethanol oxidation corresponds to the analysis of CA data in Fig. 10.

Cyclic voltammograms (CVs) of consecutive 400 cycles were measured in 1.0 mol L^{-1} NaOH $+ 0.5$ mol L^{-1} ethanol at a scan rate of 100 mV s^{-1} to further study the electrocatalytic stability of the $Pd_7Ag_2Sn_2$/CNT sample for ethanol oxidation as indicated in Fig. 12. It is clearly observed that the anodic peak current density of the sample during the forward scan decreases with the increase of cyclic sweeping number in the range of the 1st to the 50th cycle, which is attributed to the consumption of ethanol near the catalyst surface with the increase of scan time. The anodic peak current density on the forward-going scan for the 50th cycle is 89% of that for the 1st cycle. On the other hand, the anodic current density after the 50th cycle only exhibits a slight drop with the increase of the cycles, showing that a relatively steady electro-oxidation of ethanol on the $Pd_7Ag_2Sn_2$/CNT is reached. The anodic peak current density for the 400th cycle keeps 75% of that for the 1st cycle and 97% of that for the 300th cycle. Results show that this catalyst presents higher electroactivity stability for ethanol oxidation.

Fig. 11 a Electrochemical impedance spectra of the samples in 1.0 mol L^{-1} NaOH in the presence of 0.5 mol L^{-1} ethanol at -0.35 V. Dots and corresponding lines present the experimental data and fitting values respectively. **b** The equivalent electric circuit compatible with the Nyquist diagrams. *Rct* charge transfer resistance, *Rs* electrolyte resistance, *Q* constant phase element (CPE), *C* capacitance, *R3* resistance of the oxidation of the intermediates produced from alcohol oxidation
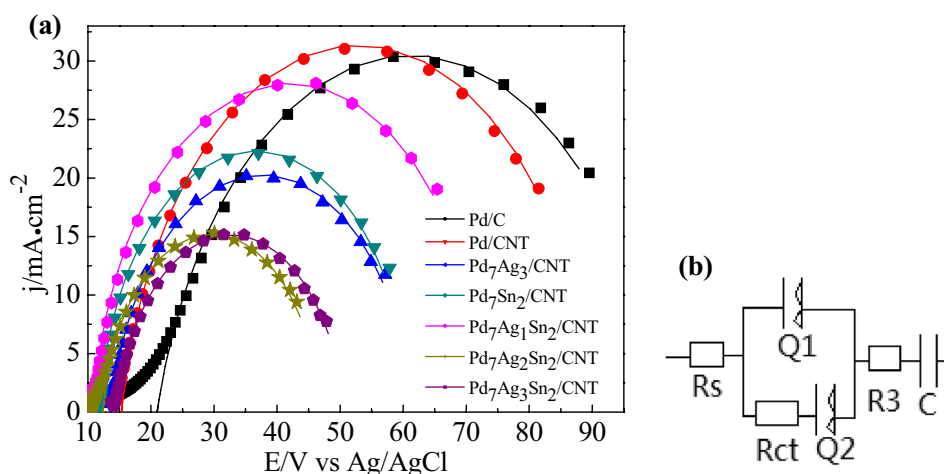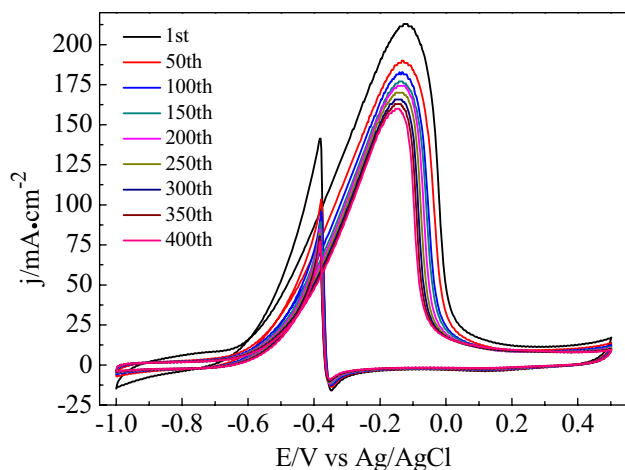
Fig. 12 400 consecutive sweeps of cyclic voltammograms on the $Pd_7Ag_2Sn_2$/CNT sample in 1 mol L^{-1} NaOH containing 0.5 mol L^{-1} ethanol at a scan rate of 50 mV s^{-1}
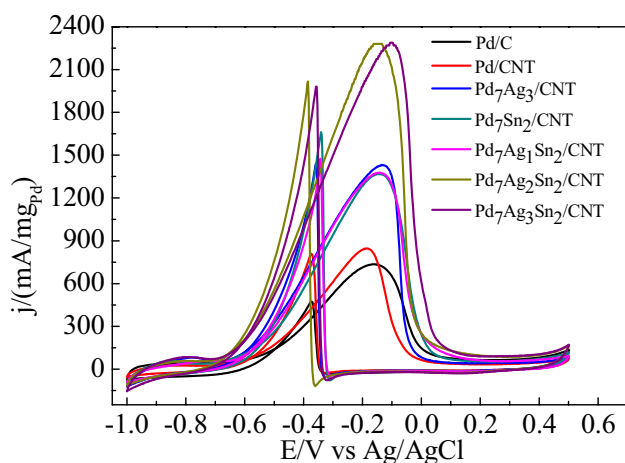
Fig. 13 Cyclic voltammograms based on the Pd mass current density from Fig. 6

In order to further investigate the Pd usage efficiency in the prepared catalysts for ethanol oxidation, the cyclic voltammograms where the current density is referenced against the Pd mass loading are presented in Fig. 13 from Fig. 6. It can be seen that the anodic peak current density during the forward-going scan on the Pd/C, Pd/CNT, Pd_7Ag_3/CNT, Pd_7Sn_2/CNT, $Pd_7Ag_1Sn_2$/CNT, $Pd_7Ag_2Sn_2$/CNT and $Pd_7Ag_3Sn_2$/CNT catalysts is 0.74, 0.86, 1.44, 1.37, 1.38, 2.29 and 2.30 A mg^{-1}, respectively. Compared to the Pd mass current density of the reported PdCuSn/CNT (0.87 A mg^{-1}) [25] and PdAuNi/C (1.41 A mg^{-1}) [42], $Pd_7Ag_2Sn_2$/CNT and $Pd_7Ag_3Sn_2$/CNT catalysts prepared in this work display much high Pd usage efficiency for ethanol oxidation. In consideration of the little difference in the electrochemical active surface areas of the prepared catalysts according to

Fig. 5, it can be reasonably inferred that the high mass current density of $Pd_7Ag_2Sn_2$/CNT and $Pd_7Ag_3Sn_2$/CNT catalysts for ethanol oxidation would be mainly ascribed to the synergetic effect between Pd and Ag/Sn.

4 Conclusion

In this work, Pd/CNT, binary Pd–Ag/CNT and ternary Pd–Ag–Sn/CNT nanocatalysts were prepared by the conventional $NaBH_4$ reduction method. SEM images presented that catalyst particles of the $Pd_7Ag_2Sn_2$/CNT were uniformly dispersed on the surface of CNTs. And this catalyst was confirmed to have smaller particles average diameter (2.4 nm) and narrow size distributions (1–6 nm) by the TEM characterization. Among the catalysts investigated, ternary $Pd_7Ag_2Sn_2$/CNT catalyst exhibits the best electrochemical activity towards the oxidation of ethanol. The current density towards ethanol oxidation can be achieved 187.5 mA cm^{-2} in alkaline medium and the mass activity is up to 2.29 A mg^{-1} (Pd), which is much higher than that of the Pd/C and Pd/CNT. The excellent electrochemical activity of ternary $Pd_7Ag_2Sn_2$/CNT catalyst should derive from the bi-functional mechanism of Pd–Ag alloy and the presence of SnO_2, which can not only absorb more OH^- on the surface of the catalyst but also rapidly remove the carbon reactive intermediates produced during the oxidation of ethanol and timely release the active sites of Pd, leading to the enhancement of the overall ethanol oxidation kinetics. Results imply that ternary Pd–Ag–Sn catalyst may be a very promising anodic electrocatalyst in the application of direct alkaline ethanol fuel cells.

Compliance with Ethical Standards

Conflict of interest All contributing authors certify that they have no affiliations with or involvement in any organization or entity with any financial or non-financial interest in the subject matter contained in this manuscript.

References

1. Dai L, Jiang LP, Abdel-Halim ES et al (2011) The fabrication of palladium hollow sphere array and application as highly active electrocatalysts for the direct oxidation of ethanol. Electrochem Commun 13(12):1525–1528
2. Liu Q, Fan J, Min Y et al (2016) B, N-codoped graphene nanoribbons supported Pd nanoparticles for enhancement of ethanol electrooxidation. J Mater Chem A 4(13):4929–4933
3. Wu T, Fan J, Li Q et al (2018) Palladium nanoparticles anchored on anatase titanium dioxide-black phosphorus

hybrids with heterointerfaces: highly electroactive and durable catalysts for ethanol electrooxidation. Adv Energy Mater 8(1):1701799(1–11)

4. Safavi A, Kazemi H, Momeni S et al (2013) Facile electrocatalytic oxidation of ethanol using Ag/Pd nanoalloys modified carbon ionic liquid electrode. Int J Hydrogen Energy 38(8):3380–3386

5. Rousseau S, Coutanceau C, Lamy C et al (2006) Direct ethanol fuel cell (DEFC): electrical performances and reaction products distribution under operating conditions with different platinum-based anodes. J Power Source 158(1):18–24

6. Zhu F, Wang M, He Y et al (2014) A comparative study of elemental additives (Ni, Co and Ag) on electrocatalytic activity improvement of PdSn-based catalysts for ethanol and formic acid electro-oxidation. Electrochim Acta 148(2):291–301

7. Zhang Y, Yi Q, Chu H et al (2017) Catalytic activity of Pd-Ag nanoparticles supported on carbon nanotubes for the electro-oxidation of ethanol and propanol. J Fuel Chem Technol 45(4):475–483

8. Almeida TS, Caíque G, Silva RG et al (2017) Addition of iron oxide to Pt-based catalyst to enhance the catalytic activity of ethanol electrooxidation. J Electroanal Chem 796:49–56

9. Sun S, Jusys Z, Behm RJ (2013) Electrooxidation of ethanol on Pt-based and Pd-based catalysts in alkaline electrolyte under fuel cell relevant reaction and transport conditions. J Power Sources 231(2):122–133

10. Xu C, Shen PK, Liu Y (2007) Ethanol electrooxidation on Pt/C and Pd/C catalysts promoted with oxide. J Power Sources 164(2):527–531

11. Rizo R, Sebastián D, Lázaro MJ et al (2017) On the design of Pt-Sn efficient catalyst for carbon monoxide and ethanol oxidation in acid and alkaline media. Appl Catal B 200:246–254

12. Ruocco C, Meloni E, Palma V et al (2016) Pt-Ni based catalyst for ethanol reforming in a fluidized bed membrane reactor. Int J Hydrogen Energy 41(44):20122–20136

13. Zignani SC, Baglio V, Linares JJ et al (2013) Endurance study of a solid polymer electrolyte direct ethanol fuel cell based on a Pt-Sn anode catalyst. Int J Hydrogen Energy 38(26):11576–11582

14. Ghavidel MRZ, Videla AHAM., Specchia S et al (2017) The relationship between the structure and ethanol oxidation activity of Pt-Cu/C alloy catalysts. Electrochim Acta 230:58–72

15. Ammam M, Easton EB (2013) PtCu/C and Pt(Cu)/C catalysts: synthesis, characterization and catalytic activity towards ethanol electrooxidation. J Power Sources 222:79–87

16. Sedighi M, Rostami AA, Alizadeh E (2017) Enhanced electro-oxidation of ethanol using Pt-CeO$_2$ electrocatalyst prepared by electrodeposition technique. Int J Hydrogen Energy 42(8):4998–5005

17. Comignani V, Sieben JM, Brigante ME et al (2015) Carbon supported Pt-NiO nanoparticles for ethanol electro-oxidation in acid media. J Power Sources 278(3):119–127

18. Takahashi H, Sagihara M, Taguchi M (2014) Electrochemically reduced Pt oxide thin film as a highly active electrocatalyst for direct ethanol alkaline fuel cell. Int J Hydrogen Energy 39(32):18424–18432

19. Cai J, Huang Y, Guo Y (2013) Bi-modified Pd/C catalyst via irreversible adsorption and its catalytic activity for ethanol oxidation in alkaline medium. Electrochim Acta 99(6):22–29

20. Alvarenga GM, Gallo IBC, Villullas HM (2017) Enhancement of ethanol oxidation on Pd nanoparticles supported on carbon-antimony tin oxide hybrids unveils the relevance of electronic effects. J Catal 348:1–8

21. Wang J, Cheng N, Banis MN et al (2015) Comparative study to understand the intrinsic properties of Pt and Pd catalysts for methanol and ethanol oxidation in alkaline media. Electrochim Acta 185:267–275

22. Chen Y, Chen M, Shi J et al (2016) Pd nanoparticles on Co nanofilms as composite electrocatalysts for ethanol oxidation in alkaline solution. Int J Hydrogen Energy 41(38):17112–17117

23. Rostami H, Rostami AA, Omrani A (2016) An electrochemical method to prepare of Pd/Cu$_2$O/MWCNT nanostructure as an anode electrocatalyst for alkaline direct ethanol fuel cells. Electrochim Acta 194:431–440

24. Liu Q, Jiang K, Fan J et al (2016) Manganese dioxide coated graphene nanoribbons supported palladium nanoparticles as an efficient catalyst for ethanol electrooxidation in alkaline media. Electrochim Acta 203:91–98

25. Zhu F, Ma G, Bai Z et al (2013) High activity of carbon nanotubes supported binary and ternary Pd-based catalysts for methanol, ethanol and formic acid electro-oxidation. J Power Sources 242(22):610–620

26. Savadogo O, Lee K, Oishi K et al (2004) New palladium alloys catalyst for the oxygen reduction reaction in an acid medium. Electrochem Commun 6(2):105–109

27. Zhang Y, Yi Q, Zou T et al (2017) In situ deposition of Pd nanoparticles on carbon paper and their electroactivity for ethanol oxidation. Ionics 23:3169–3176

28. Yi Q, Chen Q (2015) In situ preparation and high electrocatalytic activity of binary Pd-Ni nanocatalysts with low Pd-loadings. Electrochim Acta 182:96–103

29. Yi Q, Chu H, Chen Q et al (2015) High performance Pd, PdNi, PdSn and PdSnNi nanocatalysts supported on carbon nanotubes for electrooxidation of C2-C4 alcohols. Electroanalysis 27(2):388–397

30. Wang X, Ma G, Zhu F et al (2013) Preparation and characterization of micro-arc-induced Pd/TM (TM = Ni, Co and Ti) catalysts and comparison of their electrocatalytic activities toward ethanol oxidation. Electrochim Acta 114(24):500–508

31. Modibedi RM, Masombuka T, Mathe MK (2011) Carbon supported Pd-Sn and Pd-Ru-Sn nanocatalysts for ethanol electro-oxidation in alkaline medium. Int J Hydrogen Energy 36(8):4664–4672

32. Geraldes AN, Silva DFD, Silva JCMD et al (2015) Palladium and palladium-tin supported on multi wall carbon nanotubes or carbon for alkaline direct ethanol fuel cell. J Power Sources 275:189–199

33. Ramulifho T, Ozoemena KI, Modibedi RM et al (2013) Electrocatalytic oxidation of ethylene glycol at palladium-bimetallic nanocatalysts (PdSn and PdNi) supported on sulfonate-functionalised multi-walled carbon nanotubes. J Electroanal Chem 692:26–30

34. Maiyalagan T, Scott K (2010) Performance of carbon nanofiber supported Pd-Ni catalysts for electro-oxidation of ethanol in alkaline medium. J Power Sources 195(16):5246–5251

35. Zhang Z, Xin L, Sun K et al (2011) Pd-Ni electrocatalysts for efficient ethanol oxidation reaction in alkaline electrolyte. Int J Hydrogen Energy 36(20):12686–12697

36. Qi Z, Geng H, Wang X et al (2011) Novel nanocrystalline PdNi alloy catalyst for methanol and ethanol electro-oxidation in alkaline media. J Power Sources 196(14):5823–5828

37. Nguyen ST, Law HM, Nguyen HT et al (2009) Enhancement effect of Ag for Pd/C towards the ethanol electro-oxidation in alkaline media. Appl Catal B 91(1–2):507–515

38. Oliveira MC, Rego R, Fernandes LS et al (2011) Evaluation of the catalytic activity of Pd-Ag alloys on ethanol oxidation and oxygen reduction reactions in alkaline medium. J Power Sources 196(15):6092–6098

39. Jo YG, Kim SM, Kim JW et al (2016) Composition-tuned porous Pd-Ag bimetallic dendrites for the enhancement of ethanol oxidation reactions. J Alloys Compd 688:447–453

40. Jongsomjit S, Prapainainar P, Sombatmankhong K (2016) Synthesis and characterisation of Pd-Ni-Sn electrocatalyst for use in direct ethanol fuel cells. Solid State Ionics 288(5):147–153

41. Mao H, Wang L, Zhu P et al (2014) Carbon-supported PdSn-SnO$_2$ catalyst for ethanol electro-oxidation in alkaline media. Int J Hydrogen Energy 39(31):17583–17588

42. Dutta A, Datta J (2013) Outstanding catalyst performance of PdAuNi nanoparticles for the anodic reaction in an alkaline direct ethanol (with anion-exchange membrane) fuel cell. J Phys Chem C 116(49):25677–25688

43. Chetty R, Kundu S, Xia W et al (2009) PtRu nanoparticles supported on nitrogen-doped multiwalled carbon nanotubes as catalyst for methanol electrooxidation. Electrochim Acta 54(17):4208–4215

44. Hameed RMA (2017) Facile preparation of Pd-metal oxide/C electrocatalysts and their application in the electrocatalytic oxidation of ethanol. Appl Surf Sci 411:91–104

45. Kakaei K, Dorraji M (2014) One-pot synthesis of palladium silver nanoparticles decorated reduced graphene oxide and their application for ethanol oxidation in alkaline media. Electrochim Acta 143:207–215

46. Li SS, Wang AJ, Hu YY et al (2014) One-step, seedless wet-chemical synthesis of gold@palladium nanoflowers supported on reduced graphene oxide with enhanced electrocatalytic properties. J Mater Chem A 2(43):18177–18183

47. Liang ZX, Zhao TS, Xu JB et al (2009) Mechanism study of the ethanol oxidation reaction on palladium in alkaline media. Electrochim Acta 54(8):2203–2208

48. Sekol RC, Carmo M, Kumar G et al (2013) Pd-Ni-Cu-P metallic glass nanowires for methanol and ethanol oxidation in alkaline media. Int J Hydrogen Energy 38(26):11248–11255

49. Lee YW, Han SB, Park KW (2009) Electrochemical properties of Pd nanostructures in alkaline solution. Electrochem Commun 11(10):1968–1971

50. Wei YC, Liu CW, Kang WD et al (2011) Electro-catalytic activity enhancement of Pd-Ni electrocatalysts for the ethanol electro-oxidation in alkaline medium: the promotional effect of CeO_2 addition. J Electroanal Chem 660(1):64–70

51. Fu S, Zhu C, Du D et al (2015) Facile one-step synthesis of three-dimensional Pd-Ag bimetallic alloy networks and their electro-catalytic activity toward ethanol oxidation. ACS Appl Mater Interfaces 7(25):13842–13848

52. Mukherjee P, Bagchi J, Dutta S et al (2015) The nickel supported platinum catalyst for anodic oxidation of ethanol in alkaline medium. Appl Catal A 506(1):220–227

53. Yi Q, Sun L, Liu X et al (2013) Palladium-nickel nanoparticles loaded on multi-walled carbon nanotubes modified with β-cyclodextrin for electrooxidation of alcohols. Fuel 111:88–95

Affiliations

Yuanyuan Zhang[1] · Qingfeng Yi[1] · Zhongliang Deng[1] · Xiulin Zhou[1] · Huidong Nie[1]

Yuanyuan Zhang
1432195936@qq.com

[1] School of Chemistry and Chemical Engineering, Hunan University of Science and Technology, Xiangtan, Hunan 411201, China